Gaining insight into the determinants of mortality in hospitalized severely malnourished children

Versloot, Chris

DOI:
10.33612/diss.193369178

CHAPTER 6

Organoids as a model to study intestinal and liver dysfunction in severe malnutrition

Christian J. Versloot*, José M. Horcas-Nieto*, Miriam Langelaar-Makkinje, Albert Gerding, Tjasso Blokzijl, Mirjam H. Koster, Mirjam Baanstra, Robert P. Coppes, Sven C.D. van IJzendoorn, Peter Kim, Robert H.J. Bandsma, Barbara M. Bakker

* These authors contributed equally to this work

Manuscript in preparation

Abstract

Severely malnourished children face high mortality rates during treatment in hospital. Hepatic and intestinal dysfunction are common in this population with negative impacts on their survival, but the pathophysiological mechanisms are still largely unclear. We aimed to develop and characterize translational organoid models of severe malnutrition of the liver and the intestine. We show that amino-acid deprivation in organoids recapitulates organ-specific manifestations of severe malnutrition such as hepatic steatosis and intestinal barrier dysfunction. We further demonstrate that functional changes were accompanied by reduced mitochondrial and peroxisomal proteins, which could mostly be restored by the re-supplementation of amino acids or pharmacological interventions with rapamycin or fenofibrate. Restoration of protein levels aligned with signs of improved peroxisomal fatty acid oxidation in hepatic organoids and increased tight junction protein claudin-3 in intestinal organoids. Taken together, we established two organoid models that can be used to gain mechanistic insights and to test potential treatments for intestinal and hepatic dysfunction in severe malnutrition.

Introduction

The discovery of organoids has opened new possibilities for studying diseases, modelling cell development and applying them as therapeutic tools[1–4]. Their three dimensional and proliferative nature grants them the ability to maintain many of their organ functions, which makes them a physiologically relevant system to study diseases[5]. Organoids have been used to study organ-specific metabolism[6,7] and to investigate the effect of nutrients on organ homeostasis[8]. Here, we present organoids as a tool to study the impact of severe macronutrient deficiency on organ function, investigate the role of organelle homeostasis, and study the effect of putative therapeutic compounds.

Nutritional deficiencies compromise organ function and disrupt cellular metabolism[9]. Children with severe malnutrition present with the most severe form of macronutrient deficiency. In developing countries low-protein diets are common, as staple foods are often high in carbohydrates and relatively low in protein (e.g. maize), which is thought to contribute to the development of severe malnutrition[10]. Severely malnourished children face high mortality rates when admitted to hospital for treatment of acute, mostly infectious, illnesses (e.g. 23-46% in African hospitals)[11–14]. These children often show signs of hepatic dysfunction (e.g. hypoglycaemia) and intestinal dysfunction (e.g. diarrhoea), both of which have negative impacts on their survival[15–18]. Clinical studies have provided some insight into the pathophysiology of the above mentioned impairments in severe malnutrition and suggest that disrupted cellular metabolism may play a key role. Data from severely malnourished children suggests that fat accumulation, referred to as hepatic steatosis, is caused by impaired lipid oxidation rather than impaired secretion of lipids[19,20]. This is supported by post-mortem EM images that revealed dysmorphic mitochondria and a decreased number of peroxisomes, which are two of the main lipid-oxidation organelles[21]. Few studies have also reported mitochondrial morphological changes in the small intestine of severely malnourished children[22–25], but their involvement in intestinal dysfunction in severe malnutrition has not been studied. Yet, a growing body of evidence points towards a pivotal role of mitochondria in maintaining intestinal homeostasis[26–28]. Further insight into the underlying mechanisms is hindered by the invasive nature of the techniques required to obtain samples (e.g. biopsies) in this vulnerable patient population living in low-resource settings.

To overcome these limitations, animal models of severe malnutrition have been developed and used to unravel the role of organelle dysfunction in hepatic steatosis. Data from low-protein fed rodents supported the existence of a link between loss of peroxisomes, impaired mitochondrial function and the development of hepatic steatosis in severe

malnutrition[29,30]. A role of peroxisomes and mitochondria in intestinal dysfunction due to severe malnutrition has not yet been described. However, for a more in-depth analysis of organelle dynamics and the testing of potential interventions in a high-throughput approach, in vitro models may be more suitable. In cultured cells, amino acid deprivation can lead to peroxisomal degradation[29] and altered mitochondrial respiration[31,32]. Yet, these two-dimensional cell cultures are less suitable to extrapolate to organ function. Organoids have the advantages of cell culture – easy sampling and control of nutrient concentrations – while maintaining some essential characteristics of the corresponding organ[33,34].

The aim of this study was to develop and characterize translational organoid models of severe malnutrition of the liver and the intestine. Amino-acid deprivation in organoids compromised both hepatic function and intestinal structure and function in a similar way as found in vivo with a low-protein diet. Functional changes were accompanied by reduced mitochondrial and peroxisomal proteins, which could mostly be restored by the re-supplementation of amino acids or pharmacological interventions with rapamycin or fenofibrate. Restoration of protein levels aligned with signs of improved peroxisomal fatty acid oxidation in hepatic organoids and increased tight junction protein claudin-3 in intestinal organoids. We conclude that organoid models are suitable to elucidate pathophysiological processes involved in severe malnutrition and to test novel therapeutic interventions.

Methods

Animals

Crypts from the small intestine and ductal fragments from the liver were isolated from male C57BL/6J mice between 3 to 5 weeks of age (Jackson Laboratory, Bar Harbor, ME, USA). Ethical approval was obtained from the Central Authority for Scientific Procedures on Animals (CCD) of the Netherlands and from the University of Groningen Ethical Committee for Animal Experiments (Animal Use Protocol Number: 171504-01-001/3).

Intestinal crypts isolation and intestinal organoids culture

The small intestine was dissected and divided in three sections: from proximal to distal, the duodenum, jejunum and ileum. The jejunum was used to generate organoids according to a previously described protocol[1]. In short, the jejunum was cut open longitudinally, washed with ice-cold PBS and scraped to remove the villi. The tissue was cut in smaller pieces and incubated with 2.5 mM EDTA in PBS for 30 minutes at 4°C. Next, the EDTA

was removed and fresh, ice-cold PBS was added. Crypts were released from the tissue pieces by vigorously shaking. Fractions were centrifuged at 200 g for 5 minutes at 4°C. The pellet was resuspended in advanced DMEM/F12 (Thermo Fisher Scientific, Rockford, IL, USA) and centrifuged at 120 g for 5 minutes at 4°C. Crypts (pellet) were resuspended in Matrigel (Corning, NY, USA) and plated in 24-well plates. After polymerization of Matrigel, domes were overlaid with 500 µl complete culture medium. Intestinal organoids were kept in complete culture medium (CCM) consisting of Advanced DMEM/F12 containing 10mM HEPES, 1% (v/v) GlutaMax and 1% (v/v) Penicillin-Streptomycin (all Thermo Fisher Scientific) supplemented with N-2 Supplement (Invitrogen, CA, USA), B-27 Supplement (Invitrogen), 1.25 mM N-Acetylcysteine (Sigma Aldrich, MO, USA), 10% Rspondin Conditioned Medium (provided by Calvin J. Kuo), 50 ng/ml EGF (Peprotech, NJ, USA) and 100 ng/mL Noggin (Peprotech). Medium was changed every 2-3 days. Intestinal organoids were passaged every 5-7 days.

Isolation of murine biliary duct fragments and culture of liver organoids

Ductal fragments from the liver were isolated following the established protocol by Broutier et al.[35] Biliary duct fragments were kept in culture expansion medium consisting of Advanced DMEM/F12 supplemented with 10mM HEPES, 1% (v/v) GlutaMax, 1% (v/v) Penicillin-Streptomycin (all Gibco), 1% B-27 Supplement (Invitrogen) 1% N-2 Supplement (Invitrogen), 10mM Nicotinamide (Sigma Aldrich), 1.25mM N-Acetylcysteine (Sigma Aldrich), 10% RSpondin Conditioned Medium (provided by Calvin J. Kuo), 30% Wnt3a CM (provided by Hans Clevers), 100 ng/ml Noggin (Petrotech) 50 ng/ml HGF (Peprotech), 100 ng/ml FGF-10 (Peprotech), 50 ng/ml EGF (Peprotech), 10nM Leu-gastrin. Three days after the isolation Noggin and Wnt3a CM were removed from the medium. The medium was changed every 2-3 days until day 14. The organoids were then passaged and kept in culture. Liver organoids were passaged every 6-7 days.

Liver progenitor organoids were differentiated into hepatocyte organoids following the previously published method[35]. After three days in expansion medium, organoids were transferred to differentiation medium which consisted of Advanced DMEM/F12 supplemented with 10mM HEPES, 1% (v/v) GlutaMax, 1% (v/v) Penicillin-Streptomycin (all Thermo Fisher Scientific), 1% B-27 Supplement (Invitrogen) 1% N-2 Supplement (Invitrogen), 1 mM N-Acetylcysteine (Sigma Aldrich), 100 ng/ml FGF-10 (Peprotech), 50 ng/ml EGF (Peprotech), 10nM Leu-gastrin (Sigma Aldrich), 50nM A-83-01 (Tocris, Bristol, UK) and 10uM DAPT (Sigma Aldrich).

Malnutrition in organoids using amino acid starvation

To mimic malnutrition in organoids, a custom-made amino acid free Advanced DMEM/F12 was used (Invitrogen). Apart from this amino acid free DMEM, the formulation of the culture media was identical as described above for the respective organs. Intestinal organoids were grown in complete culture medium for three days after passage before being placed in low amino acid culture medium for 48 hours. Liver progenitor organoids were grown in complete expansion medium for 3 days after passage before being placed in differentiation medium until day 13. At day 13 the already mature hepatic organoids were placed in low amino acid differentiation medium for two more days prior to collection of supernatant and organoids.

Amino acid re-supplementation studies

Intestinal organoids were grown in complete culture medium until three days after the passage, then placed in amino acid-free medium for 48 hours, followed by re-supplementation of amino acids for 48 hours respectively.

Hepatic organoids were grown in complete differentiation medium until day 12. From day 12 to day 14 they were grown in amino acid-free medium. At the end of day 14 the organoids were placed back in complete differentiation medium until the end of day 16. The supernatant from the organoids was collected every 24 hours for serial assessment of albumin production.

Therapeutic interventions

Intestinal organoids were grown in complete culture medium until three days after the passage, then placed in amino acid-free medium for 48 hours that was supplemented with rapamycin (Sigma Aldrich, MO, USA) at a final concentration of 2nM.

Hepatic organoids were grown in complete differentiation medium until day 12. From day 12 to day 14 they were grown in amino acid-free medium supplemented with fenofibrate (Sigma Aldrich) at a final concentration of either 10 or 100μM, as indicated.

Amino acid measurements

Amino acid profiles were measured by GC/MS (Agilent 9575C series GC/MSD, Agilent Technologies, Amstelveen, The Netherlands) as previously described[36].

RNA isolation, reverse transcription and quantitative real-time qPCR

Total RNA was extracted from organoids using the commercially available RNeasy Mini Kit (Qiagen, Hilden, Germany) according to the manufacturer's instructions. RNA quality and quantity was determined with NanoDrop (NanoDrop Technologies, Wilmington, DE, USA). Reverse transcription was completed with the M-MLV Reverse Transcriptase (200 U/µL) (invitrogen) according to the manufacturer's instructions. qPCR reactions were performed using FastStart Universal SYBR Green Master (Rox) (Sigma Aldrich) in 384 well format in duplicate with 20 ng total RNA per well in a QuantStudio 7 Flex (Thermo Fisher Scientific). All primers sequences (Integrated DNA technologies Inc., Coralville, IA, USA) are listed in **Supplementary Table 1**. Peptidylprolyl isomerase A (cycophilin A)(PPIA) served as endogenous control, as expression was stable between experimental groups and was used for normalization. Relative expression was calculated using the ΔΔC(t) method relative to the control organoids.

Imaging of the liver and intestinal organoids and processing of the images

Organoid cultures were followed over time with an AxioObserver Z1 compound microscope (Carl Zeiss), 2.5x and 5x objectives and an AxioCam MRm3 CCD camera (Carl Zeiss). Raw images were processed using the ZEN 3.1 blue edition software. The number and size of organoids were assessed in the whole well. A set of 25 organoids were manually counted in each well, tracked over time and measured throughout the different time points.

Albumin measurement

Supernatant from the hepatic organoid cultures was collected every 24 hours starting from day 12 of the differentiation until day 16 and was immediately stored at -20°C. The concentration of albumin in the supernatant was measured using the mouse albumin ELISA kit (Abcam, Cambridge, UK) according to the manufacturer's instructions in the Synergy H4 Hybrid Microplate Reader (BioTek Instruments Inc., VT, USA).

Triglyceride measurement

Organoids were collected in 1X TBS in MiliQ water. Fat was extracted using chloroform-methanol in a 2:1 ratio. Quantitative determination of hepatic triglycerides was done with

the DiaSys Triglyceride FS kit (Holzheim, Germany, Cat #157109910971). Results were normalized for protein content.

BODIPY Staining

Organoids were fixed in 4% PFA for 1 hour at 37°C. Permeabilization and staining were done simultaneously in a CLMS buffer (PBS, 3% BSA, 10mM glycine) containing 0.1% saponine, 15μM BODIPY (Thermo Fisher Scientific) and 5μM Hoechst (Thermo Fisher Scientific) for 1 hour at room temperature. The organoids were washed with PBS and images were acquired with an AxioObserver Z1 compound microscope (Carl Zeiss), 40X objective and AxioCam Mrm3 CCD camera (Carl Zeiss).

Permeability measurement (FITC)

Permeability of intestinal organoids was assessed using fluorescence markers. Organoids were incubated with FITC-dextran 4kDa or 10kDa (TdB consultancy, Uppsala, Sweden) at a final concentration of 1.25μM in their respective advanced DMEM/F12 (with or w/o amino acids) for 30 minutes at room temperature. Next, organoids were gently washed 5-10 times with PBS to remove any non-specific binding. The degree of accumulation in the lumen of the organoid served as a measure for permeability. All organoids in each well were imaged with an AxioObserver Z1 compound microscope (Carl Zeiss), 2.5x or 10x objective and AxioCam MRm3 CCD camera (Carl Zeiss). ZEN 3.1 blue edition software was used to measure the fluorescence in the organoid lumen. To correct for differences in background fluorescence, the intensity was measured in three different areas around the organoid. The mean intensity measured in three squares around the organoid was subtracted from the luminal fluorescence.

Immunoblotting

For Western blotting, the protocol was based on a previously published paper[37]. Organoids were collected using the respective cold Advanced DMEM/F12 (with or w/o amino acids) and kept on ice for 10 minutes to ensure Matrigel dissolvement. Organoids were centrifuged at 200-290G for 5 minutes followed by one wash with cold PBS. Organoids were again centrifuged and resuspended in 200uL of radio immunoprecipitation assay buffer (1% IGEPAL CA-630, 0.1% SDS, and 0.5% sodium deoxycholate in PBS) supplemented with Complete Protease Inhibitor Cocktail (Cat. No. 1186145001; Sigma-Aldrich), Phosphatase Inhibitor Cocktail 2 (Cat. No. P5726; Sigma Aldrich) and Cocktail 3 (Cat. No. P0044; Sigma Aldrich). Organoid lysates were sonicated using Sonics Vibra

cell VCX130 (Sonics & Materials inc, Newtown, USA) using a 50% amplitude four times for 10 seconds. Protein concentration was measured using Pierce BCA Protein Assay Kit (ThermoScientific, Rockford, IL, USA). All samples were adjusted to the lowest protein concentration value. Organoid lysates were then mixed with Laemli buffer (10% glycerol, 1% B-mercaptoethanol, 1.7% SDS, 62.5 mM TRIS base (pH6.8) and bromophenol blue) and heated for 10 minutes at 95°C. The percentage of acrylamide in the gels ranged from 12 to 14% depending on the size of the proteins detected. The separation was performed between 90V to 180V using a Mini-PROTEAN Tetra Vertical Electrophoresis Cell system (Cat. No. 1658029FC; Bio-Rad, CA, USA) with running buffer (0.2 M glycine, 25 mM TRIS bas, and 0.1% SDS. To transfer the protein we used polyvinylidene difluoride membranes (Cat. No. IPVH00010; Sigma Aldrich) and the PROTEAN Tetra Vertical Electrophoresis Cell system with blotting buffer (0.1 M glycine, 50 mM TRIS base, 0.01% SDS (pH 8.3) and 10% methanol) at 45V for 1h and 50 minutes. The membranes were blocked using 5% BSA in TBST for at least 20 minutes prior to incubation with primary antibodies at 4°C overnight. The antibodies and dilutions are listed in **Supplementary Table 2**. The membranes were then washed with TBST and incubated with HRP-coupled secondary antibody (goat anti-mouse and goat anti-rabbit) for at least 2 hours at room temperature. To detect, Pierce ECL Western Blotting Substrate (Cat. No. 32209; Thermo Fisher Scientific) or SuperSignal West FEMTO (Cat. No. 34095; Thermo Fisher Scientific) were used using an LAS-4000 mini camera system (GE Healthcare). Images taken with LAS-4000 mini system were exported as TIFF files and the quantification of the raw images was done using ImageQuant TL version 8.1 (GE Healthcare, IL, USA). The subtraction of the background was performed using the rolling ball method. The pixel value of all the signals were normalized to the average intensity of all the signals belonging to the same readout. Next, for liver organoids the signals were normalized to the loading control B-actin. For intestinal organoids, the signals were normalized to total protein (Simply Blue™ SafeStain, Thermo Fisher Scientific)[38] because various loading controls that were evaluated, displayed high variability between control and amino-acid starved organoids. For statistical analysis GraphPad Prism Software Version 9.00 (GraphPad Software, San Diego, California, USA) was used.

High resolution respirometry

Organoids were collected in the respective Advanced DMEM/F12 (with or w/o amino acids) at 4°C and kept on ice for 10 minutes to properly disrupt the Matrigel. After centrifugation at 200-290 g for 5 minutes at 4°C, supernatant was removed and organoids were washed with MiR05 buffer followed by another centrifugation step. Organoids were

then resuspended in 600uL of MiR05 buffer containing 110mM sucrose, 60mM potassium lactobionate, 20mM taurine, 20mM HEPES, 0.5mM EGTA, 10mM KH2PO4, 3mM MgCl2, 1mg/ml bovine serum albumin, pH 7.1.

The rate of oxygen consumption of the organoids was measured using a two-channel high-resolution Oroboros Oxygraph-2 k (Oroboros, Innsbruck, Austria) at 37°C. The oxidable substrates used in the experiments were 25uM Palmitoyl Carnitine plus 2mM Malate to stimulate the fatty acid b-oxidation. Maximal ADP-stimulated respiration was achieved by addition of 1mM ADP (state 3). Next, basal respiration (state 4) was determined using Oligomycin to block ATP synthase. Finally, 0.5mM FCCP was added in order to study the oxygen consumption during uncoupled respiration (State U). Oxygen consumption rates were expressed in nmol/min/mg of protein.

Branched chain fatty acid and very long chain fatty acid measurements

Mature hepatic organoids were incubated with 25µM phytol (Sigma Aldrich) for 48 hours prior to quenching in ice-cold methanol. Methanol was evaporated at 37°C under a steady stream of N_2 for 40 minutes. Next, the pellet was reconstituted in PBS. Samples were hydrolysed in two steps. First, an acid hydrolysis step was performed to release the fatty acids from the different moieties they are bound to without affecting phytanic acid. This was followed by a basic hydrolysis to convert esterified fatty acids into free fatty acids. Pentafluorobenzyl bromide (PFB-Br) was added for the derivatization. The PFB derivatives were analysed on the GC/MS (Agilent 7890/5975 inert XL GCMS System, Agilent Technologies, Amstelveen, The Netherlands) in negative chemical ionization mode (NCI). Results were normalized for protein content.

Statistical analysis

All results are expressed as mean ± standard error of the mean (SEM) or mean ± standard deviation (SD), as indicated. Group differences were assessed with repeated measures ANOVA for multiple day organoids size measurements or an ordinary one or two-way ANOVA with Tukey's post hoc multiple comparisons analyses. Statistical analysis was performed with GraphPad Prism Software Version 9.02 (Graphpad Software, San Diego, California USA). Statistical significance was given as *** P value <0.001, ** P value < 0.01 and * P value < 0.5; NS (not significant).

Results

Hepatic and intestinal organoid lines were established from mouse intestinal crypts and biliary duct fragments, respectively. To mimic the effect of a low-protein diet, the organoids were cultured in a medium to which no amino acids were added. Nevertheless, most amino acids were still present at low levels, presumably originating from Matrigel degradation as well as from growth factors present in the medium (**Supplementary Table 3**).

Impact of amino acid starvation on structure and function of liver organoids

Hepatocyte maturation was confirmed by the expression of hepatocyte differentiation markers such as HNF-4a, CYP1a2 and CYP3a11 (**Supplementary Figure 1**). Deprivation of amino acids up to 96 hours did not significantly affect the growth or the morphology of mature hepatic organoids (**Figure 1a,b**). In contrast, when liver progenitor organoids were exposed to the starvation medium, organoids remained smaller than control organoids (**Supplementary Figure 2**). The different response to removal of amino acids likely reflects the lower proliferative state of mature hepatic organoids as indicated by lower gene expression levels of stem cells markers (Supplementary Figure 1). Starvation of mature hepatic organoids for 48 hours substantially reduced the levels of albumin in the supernatant (**Figure 1c**). Re-supplementation of amino acids restored albumin production completely (**Figure 1c**). Furthermore, starved mature hepatic organoids showed increased fat deposition as indicated by an increase in lipid droplets (**Figure 1d**).

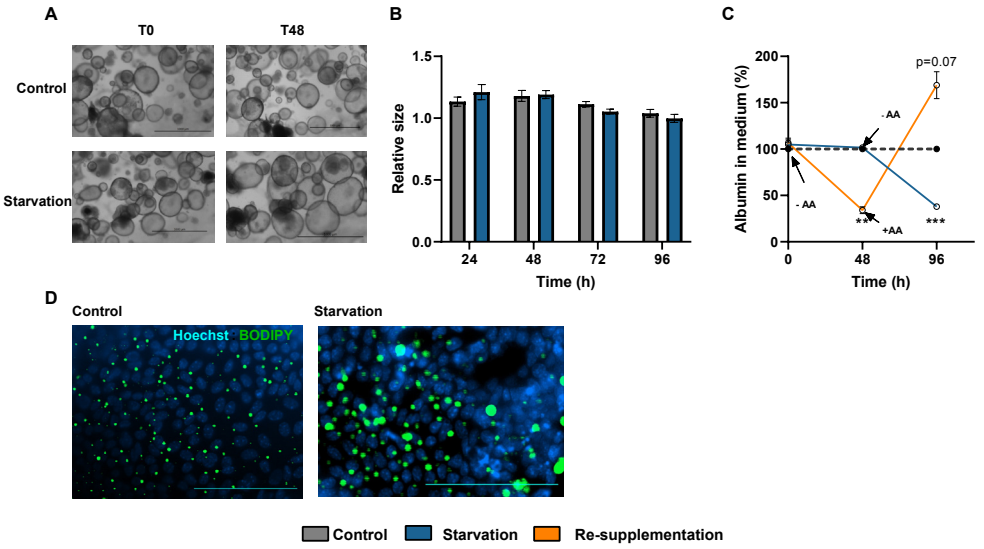

Figure 1. Amino acid starvation leads to functional changes in mature hepatic organoids without profound morphological changes. (A) Representative bright-field images of control and starved mature hepatic organoids at the start and after 48 h. Scale bar, 1 mm. **(B)** Relative size of organoids in complete culture medium (control) or amino-acid free medium (starved), expressed as size of an organoid at time point of interest divided by the size of the same organoid 24 hours earlier calculated for 25 random organoids. Data points represent 3 biological replicates, error bars indicate the SEM. **(C)** Albumin levels were measured in medium of organoids of the different experimental conditions. Albumin production is shown for control organoids (dotted line), organoids starved for amino acids from 48h to 96h (blue line), and organoids starved for amino acids from 0h to 48h and re-supplemented with amino acids from 48h to 96h (orange line). Removal of amino acids is indicated with '-AA' and re-supplementation with '+AA'. Values are normalized to the control condition of that respective time point. Data points represent 3 biological replicates, error bars indicate the SEM (*P<0.05, repeated measures analysis of variance with Tukey's post hoc test). **(D)** Representative immunofluorescence images of control and starved mature hepatic organoids (40x magnification). BODIPY was used to stain fat droplets in green, and Hoechst was used to counter stain nuclei in blue. Scale bar, 100 µm.

Impact of amino acid starvation on structure and function of small intestinal organoids

After 48 hours starvation for amino acids, intestinal organoids were significantly smaller than non-starved organoids (**Figure 2a,b and Supplementary Figure 3a**). In addition, amino-acid-starved organoids displayed crypt atrophy and had substantially fewer crypts compared to control organoids (**Figure 2c,d and Supplementary Figure 3b**). Amino-acid deprivation upregulated the expression of markers of Paneth cells (lysozyme), goblet cells (mucin-2) and enteroendocrine cells (chromogranin A), but did not affect the expression of stem cell or proliferation markers (**Supplementary Figure 4**). FITC-dextran (4 and 10kDa) leakage into the organoid lumen was increased, as indicated by increased

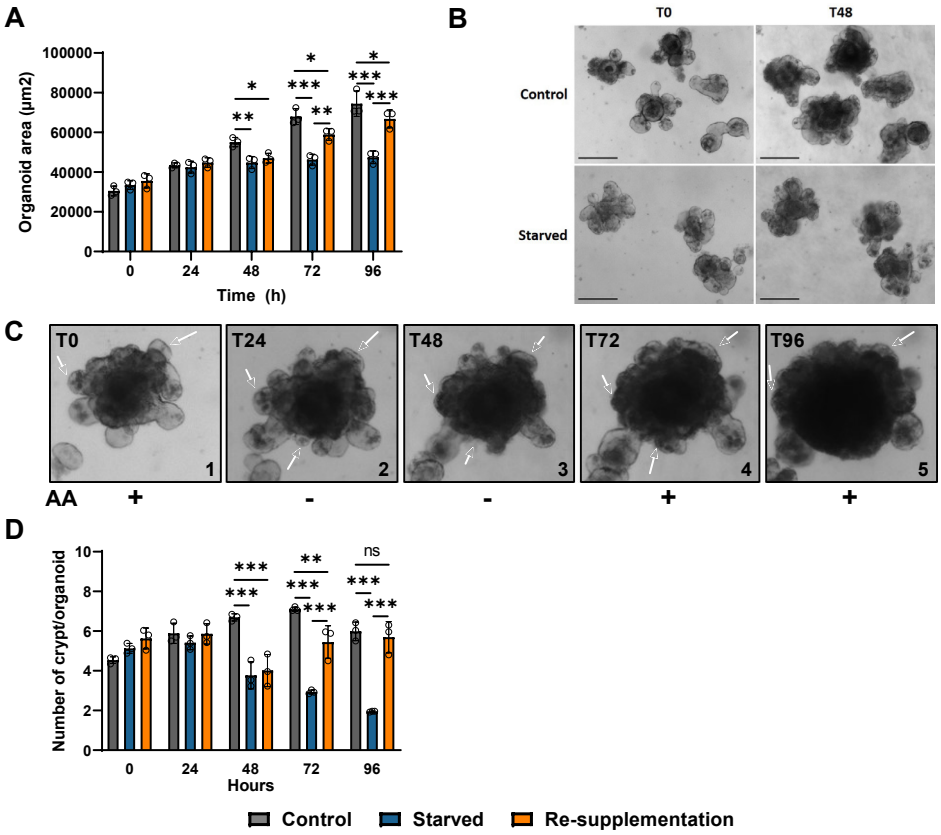

Figure 2. Amino acid deprivation induces reversible crypt atrophy, compromised growth and barrier dysfunction in intestinal organoids. (A) Organoid size over time of organoids grown in complete culture medium (control), amino-acid-free medium (starved) or amino-acid-free medium for 48 h followed by complete culture medium for 48 h (re-supplementation). Data points represent the average of 26 measured organoids in each of the 3 biological replicates, error bars indicate the SD (* P< 0.001, ** P < 0.01, * P <0.05, repeated measures analysis of variance with Tukey's post hoc test). **(B)** Representative bright-field images of control and starved intestinal organoids at the start and after 48 h. Scale bar, 200 µm. **(C)** Representative bright-field images show an individual small intestinal organoid grown in complete culture medium for 3 days (C1), switched to amino acid free medium for 48 h (C2 and C3), and then placed in complete culture medium for 48 h (C4 and C5). Arrowheads indicate individual crypt domains. **(D)** Average number of crypts per organoid over time for control, starvation and re-supplementation. Data points represent the average of 26 measured organoids in each of the 3 biological replicates, error bars indicate SD (** P < 0.01, *** P <0.001, repeated measures analysis of variance with Tukey's post hoc.

number of FITC-dextran positive organoids as well as higher luminal fluorescence, showing that amino-acid starvation compromised the intestinal barrier function (**Figure 3a-c, Supplementary figure 5**). This is consistent with *in vivo* findings[39] and was supported by reduced levels of the tight-junction protein claudin-3 (**Figure 3d**). Re-supplementation of amino acids restored organoid size, crypt numbers, claudin-3 protein level, and

expression of mucin-2 and chromogranin A, and increased stem cell markers LGR5 and Axin2 (**Figure 2a-d, Supplementary Figure 4**). Intestinal barrier function could not be properly assessed with FITC-dextran due to the high amount of content (e.g. dead cells) in the organoids lumen after 96 hours.

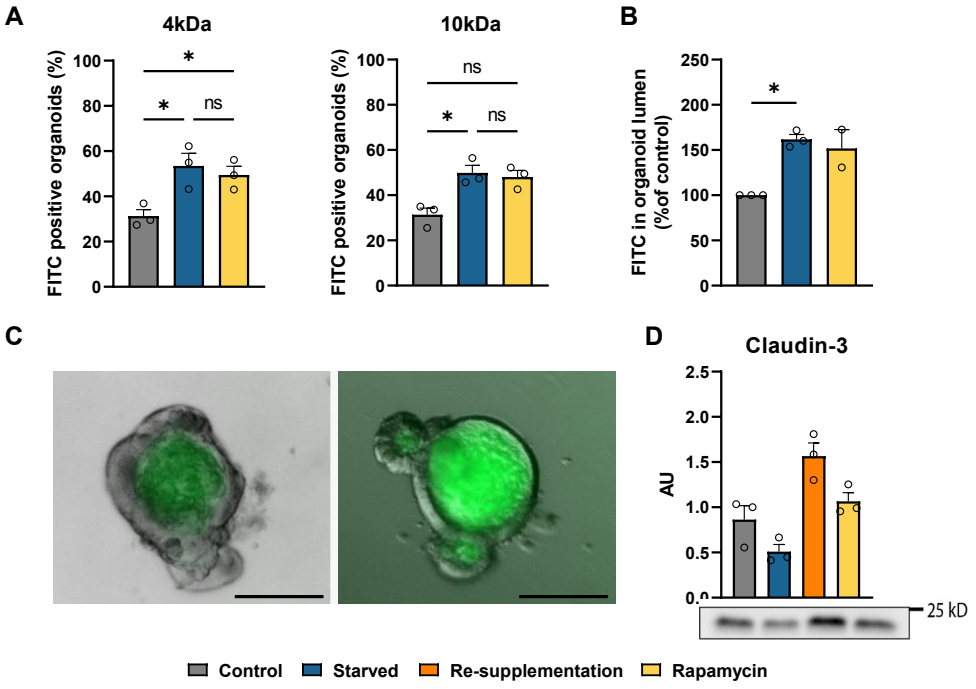

Figure 3. Amino acid deprivation induces barrier dysfunction in intestinal organoids, which may partially restored by amino-acid re-supplementation or rapamycin administration.
(A) Percentage of intestinal organoids with 4 or 10 kDa inside their lumen measured in organoids grown in complete culture medium (control), amino-acid-free medium (starved) and amino-acid-free medium supplemented with 2nM rapamycin (rapamycin). Data represents mean ± SEM from 3 biological replicates (*P<0.05, two-way ANOVA with Tukey's post hoc test). **(B)** Average luminal FITC fluorescence for control, starved and rapamycin-administered organoids. Values are normalized to control organoids. Data represent mean ± SEM from 2-4 biological replicates (*P<0.05, two-way ANOVA with Tukey's post hoc test). **(C)** Representative images for 10 kDa FITC-dextran for control and starved organoid (10x magnification). Scale bar, 100 µm **(D)** Immunoblot quantification and representative image of tight-junction protein claudin-3 relative to total protein (see methods) for the different conditions. Data represent mean ± SEM from 3 biological replicates. (*P<0.05, ** P< 0.01, Two-way ANOVA with Tukey's post-hoc test).

Amino-acid starvation reversibly reduces the levels of peroxisomal proteins in hepatic organoids

In vivo studies of rats and mice on a low protein diet showed a decline of peroxisome numbers and altered mitochondrial morphology and function in the liver[29,30]. Compromised oxidation of fatty acids by peroxisomes and mitochondria explains hepatic steatosis in these studies. We aimed to determine whether these findings could be recapitulated in amino-acid-deprived hepatic organoids.

Peroxisomal proliferator-activated receptor gamma coactivator 1-alpha (PGC1-α), an activator of peroxisomal and mitochondrial biogenesis[40], was clearly reduced in the starved condition. Also, the protein levels of PMP-70, an ATP-binding cassette transporter and a major component of the peroxisomal membrane[41], was strongly reduced upon amino acid deprivation. The same was found for the peroxisomal enzymes acyl-CoA oxidase 1 (Acox-1) and catalase (**Figure 4a, b**). With respect to mitochondria, the level of TOM-20 (a component of the 'translocase of outer membrane' (TOM) receptor complex) did not differ between control and starved conditions. HSP60, a mitochondrial matrix marker protein was slightly decreased under amino-acid-starved conditions (Figure 3b). Some complexes of the electron transport chain showed a mild reduction in starved organoids, but this was not statistically significant (Figure 4a, b). Peroxisomal fatty acid oxidation was assessed following the metabolism of phytol, a precursor of phytanic acid. Phytanic acid, pristanic acid and very-long-chain fatty acids (VLCFA) accumulated in starved organoids (Figure 5a), indicating a reduction in peroxisomal fatty acid oxidation. Mitochondrial oxygen consumption was not affected in organoids starved for 48 hours when compared to healthy controls (**Figure 5b**). We observed a small but significant increase in intracellular triglycerides (TG) in starved hepatic organoids (**Figure 5c,d**).

Re-introduction of amino acids for 48 hours following 48 hours of starvation recovered most of the peroxisomal protein levels to almost those of the control organoids (Figure 4 a,b). Levels of phytanic and pristanic acid as well as VLCFA were partially recovered but remained higher than in the controls (**Figure 5a**). Since no regulation was observed in mitochondrial protein levels, re-introduction of amino acids did not have any further effect. Intracellular TG levels were significantly lower upon re-supplementation (Figure 5d).

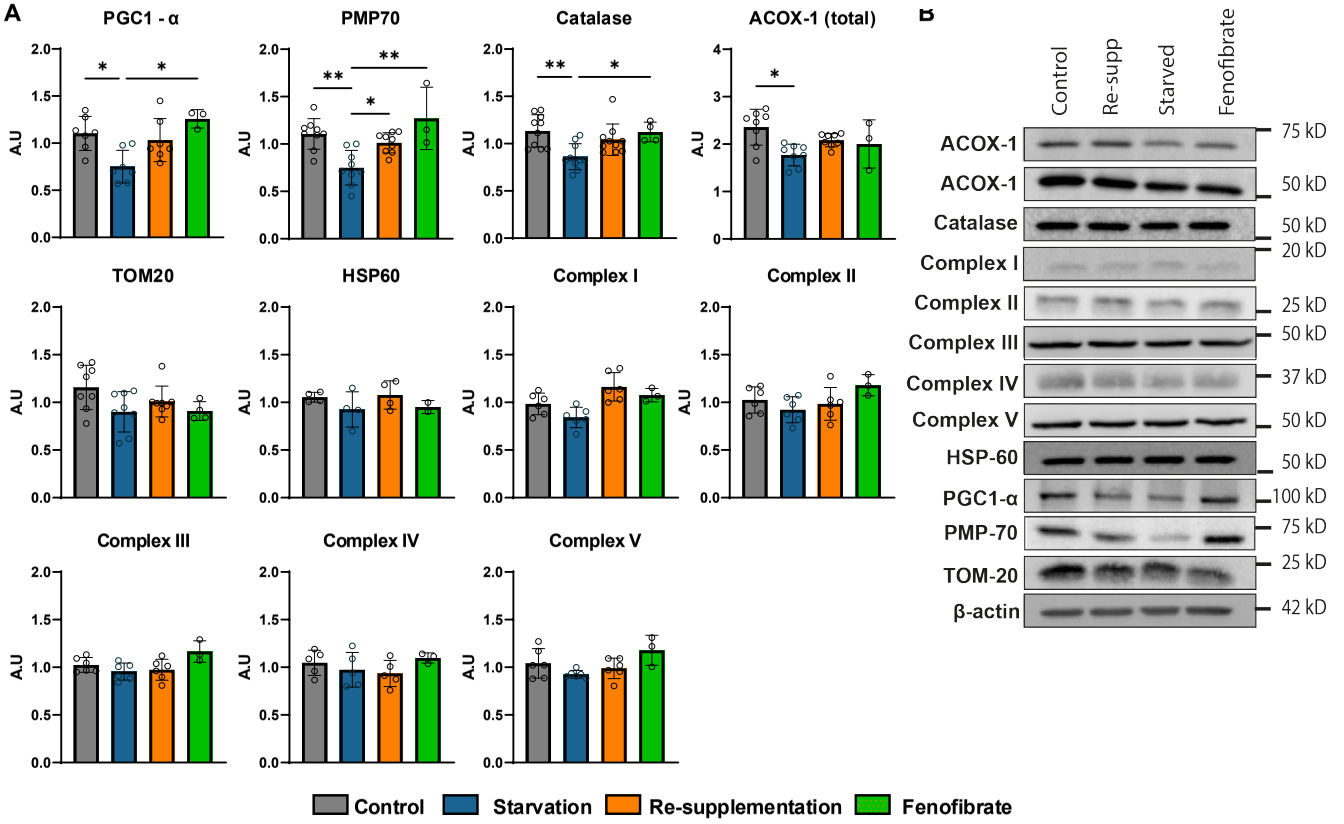

Figure 4. Impact of amino acid starvation and re-supplementation on mitochondria and peroxisomes in mature hepatic organoids. (A) Protein levels relative to β-actin. Quantification of data shown in (B). **(B)** Representative immunoblot images. Organoids were grown in complete culture medium (control), amino-acid-free medium (starved), amino-acid-free medium for 48 h followed by complete culture medium for 48 h (re-supplementation) or in amino-acid-free medium for 48 h supplemented with 100uM fenofibrate. Data represent mean ± SEM from 7-10 biological replicates and 3 biological replicates for fenofibrate treatment (*P<0.05, **P< 0.01,Two-way ANOVA with Tukey's post-hoc test).

Amino acid deprivation reversibly reduces mitochondrial and peroxisomal content in intestinal organoids

In view of the key role of mitochondria and peroxisomes in intestinal homeostasis[26,42], we also examined the effect of amino acid deprivation on these organelles in intestinal organoids. In contrast to hepatic organoids, amino acid starvation did not affect the protein level of PGC1-α (**Figure 6a,b**). The levels of the peroxisomal proteins PMP-70, ACOX-1 and catalase, were, however, all reduced in starved intestinal organoids (Figure 6a-c).

Mitochondrial marker proteins Tom-20 and Hsp60 were also downregulated by amino acid starvation (Figure 6a-c). Yet, the complexes of the electron transport chain were not affected by amino-acid starvation (Figure 6a-c). Amino acid re-supplementation normalized all peroxisomal and mitochondrial characteristics, except the level of TOM-20, which was highly increased after re-supplementation (Figure 6a-c).

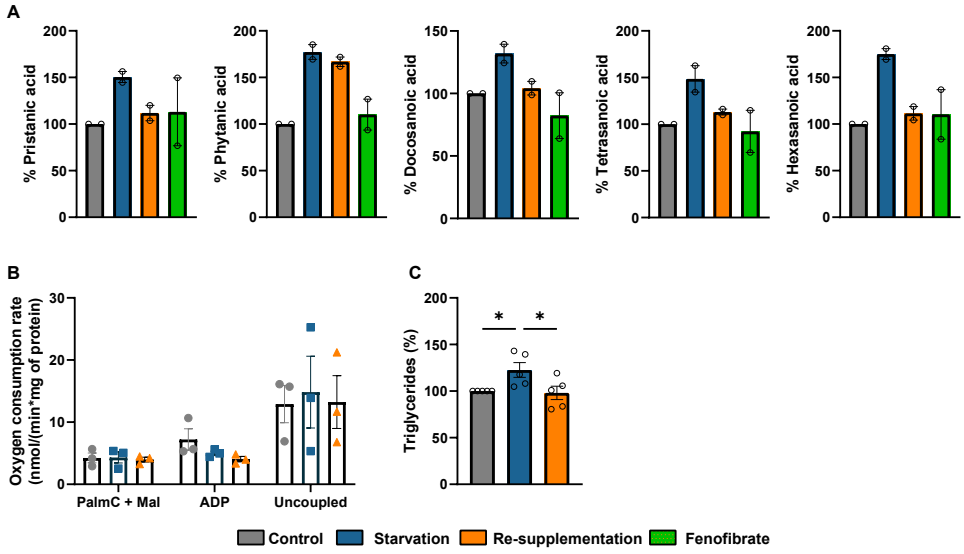

Figure 5. Impact of amino acid starvation, re-supplementation and fenofibrate on peroxisomal fatty acid oxidation and mitochondrial oxygen consumption.
(A) Levels of pristanic acid, phytanic acid and VLCFA in organoids that were grown in complete culture medium (control), amino-acid-free medium (starved), amino-acid-free medium for 48 h followed by complete culture medium for 48 h (re-supplementation) or in amino-acid-free medium for 48 h supplemented with 10 μM fenofibrate. Preliminary data represent 2 biological replicates. **(B)** Oxygen consumption rate in organoids measured as basal respiration (stimulated with Palmitoyl Carnitine and ADP), State 3 (ADP) and uncoupled respiration (FCCP). Data represent the mean ± SEM. Data represent 3 biological replicates (Two-way ANOVA with Tukey' post-hoc test) **(C)** TG levels in control, starved and re-supplemented organoids. Data points represent 5 biological replicates (*P<0.05, ordinary one-way ANOVA with Tukey's post hoc test).

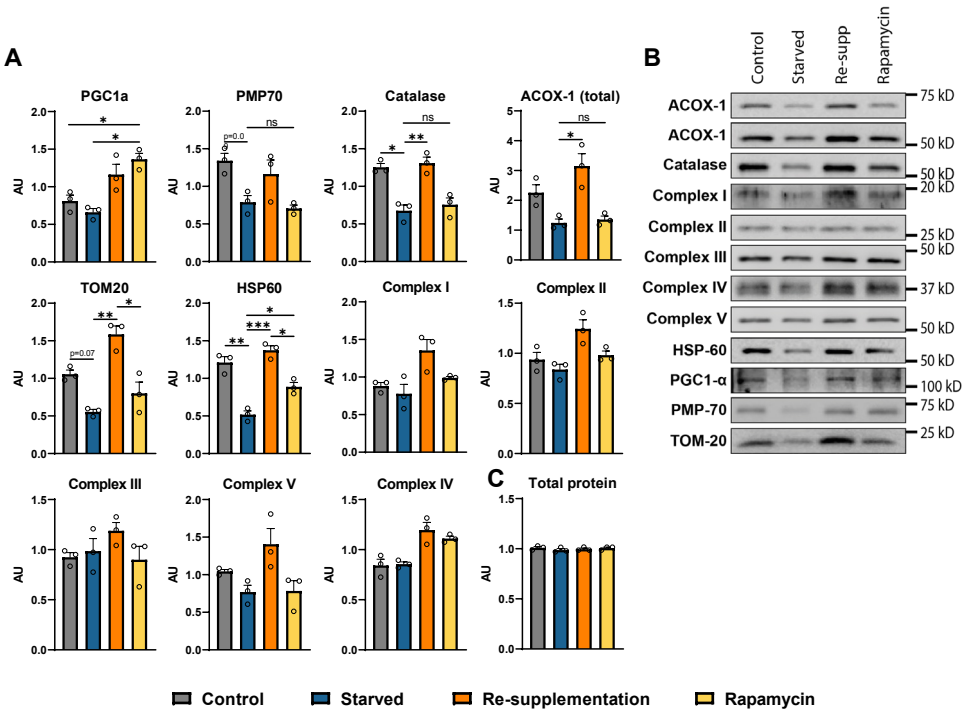

Figure 6. Impact of amino acid starvation, re-supplementation and rapamycin on mitochondria and peroxisomes in intestinal organoids.
(A) Quantification of data shown in (B). Protein levels were normalized to total protein (see methods section). **(B)** Representative immunoblot images. Organoids were grown in complete culture medium (control), amino-acid-free medium (starved), amino-acid-free medium for 48 h followed by complete culture medium for 48 h (re-supplementation) or in amino-acid-free medium for 48 h supplemented with 2nM rapamycin. Data represent mean ± SEM from 3 biological replicates (*P<0.05, ** P< 0.01, *** P<0.001, Two-way ANOVA with Tukey's post-hoc test). **(C)** Relative intensity of total protein measured in each entire lane (used for total protein normalization as explained in methods). Individual data points are shown for each biological replicate.

Interventions to preserve mitochondria and peroxisomes in starved organoids

We investigated if amino-acid-deprived organoids could be used as a model to test pharmacological interventions to preserve organ function. As a proof of principle, we tested interventions that have already been applied in animal studies. Fenofibrate, a PPAR-α agonist, was previously shown to restore peroxisomes and mitochondrial function in the liver of rats on a low protein diet[30]. When administered to amino-acid-starved mature hepatic organoids, fenofibrate increased levels of peroxisomal proteins to values similar as the controls (Figure 4a, b). In addition, fenofibrate recovered levels of phytanic and pristanic acid, as well as VLCFA to those of the controls (Figure 5a). No

regulation was observed for mitochondrial proteins. Addition of fenofibrate did not affect intracellular triglycerides levels.

We recently showed that rapamycin, a mTORC1 inhibitor, preserved intestinal barrier function and mitochondrial number and morphology in mice on a low protein diet (Chapter 5) . Likewise, in amino-acid-starved intestinal organoids, rapamycin increased the levels of mitochondrial marker proteins Tom-20 and HSP-60, although they remained lower than in control organoids (Figure 6a,b). In addition, protein levels of PGC1-α were increased in amino-acid-starved, rapamycin-treated organoids to a similar level as in amino-acid-re-supplemented organoids (Figure 6a,b). Although PGC1-α is also known as an activator of peroxisomal biogenesis, rapamycin treatment did not affect the protein levels of peroxisomal proteins (Figure 6a,b). Rapamycin treatment did, however, preserve claudin-3 protein levels in starved organoids, suggesting preserved intestinal barrier function (Figure 3d). However, rapamycin did not appear to decrease the number of FITC-dextran positive organoids (Figure 3a). As the response in rapamycin-administered organoids for the luminal fluorescence was obtained for 2 biological replicates (Figure 3b) we cannot draw any final conclusions. This experiment needs to be done for a third time to clarify whether rapamycin indeed improves intestinal barrier function.

Discussion

Advances in three-dimensional cultures, in particular organoids, have opened new avenues for the development of more physiological in vitro models of organ function and diseases[1–4]. In this paper, we presented two organoid models to study pathophysiological processes and potential treatments for intestinal and hepatic dysfunction in severe malnutrition. Organ-specific manifestations of severe malnutrition were recapitulated in amino-acid-starved organoids. Concurrent mitochondrial and peroxisomal changes largely reflect in vivo findings and were found to be organ-specific. We showed that amino-acid-starved organoids cannot only be used to gain mechanistic insights, but also to test pharmacological interventions.

Functional impact of amino acid starvation on hepatic and intestinal organoids

In mature hepatic organoids, no morphological or size changes were observed upon amino-acid starvation. This could be attributed to their low proliferative state, as indicated by lower stemness and proliferation markers than in hepatic progenitor organoids. Their functionality was, however, substantially impaired. Albumin production dropped upon

starvation, which should be expected as albumin synthesis requires amino acids as precursors and is stimulated by dietary amino acids[43]. The same was observed in low-protein fed rats[17]and severely malnourished children[44]. Moreover, enlarged fat droplets and elevated levels of branched-chain and very-long-chain fatty acids point to lipid accumulation in starved hepatic organoids. Hepatic steatosis has also been commonly observed in severely malnourished children[45] and rodents on a low-protein diet[30,46]. We did not study glucose production, even though impaired hepatic glucose production reported in severely malnourished children increases the risk of hypoglycaemia and death[15,17]. Functional glucose production has rarely been studied in organoids since glucose 6-phosphatase (G6PC) levels are typically low in vitro[47,48]. It was recently shown that organoids derived from primary hepatocytes have a higher G6PC expression[33] than organoids derived from cholangiocytes, and a normalized glycogen storage[49]. This provides a perspective to study functional glucose production in vitro.

Intestinal organoids starved for amino acids were smaller than their counterparts on complete medium, with fewer crypts and atrophy of cryptlike domains. This could point to suppressed enterocyte proliferation, which has been demonstrated in intestinal organoids deprived of glutamine, methionine or valine[50,51]. In starved organoids gene expression of stem cell and proliferation markers was not significantly reduced, but increased upon re-supplementation. This is in line with the observed re-growth of crypts. Restoration of growth and new crypt formation after amino acid re-supplementation indicate that the intestinal stem cells have the capacity to recover from prolonged amino-acid starvation. Re-growth of crypts may be attributed to rapidly cycling $Lgr5^{+}$ crypt base columnar (CBC) cells, which were previously found resilient to glutamine starvation[50]. Another possibility is the mobilization of another stem cell population referred to as quiescent 'reserve' stem cells (+4 position) that are activated upon injury to restore tissue homeostasis[52]. Moreover, de-differentiation of progenitor cells[53,54] as well as differentiated epithelial cells can contribute to repopulation of the stem cell niche[55,56]. Yet, the impact of prolonged amino-acid deprivation on intestinal stem cells and on de-differentiation has not been studied. Finally, the barrier dysfunction and reduction of claudin-3 in starved intestinal organoids was in agreement with reported findings in severely malnourished children[57–59] and in low-protein fed rodents[39] (Chapter 5).

Impact of amino acid starvation on organelle homeostasis in hepatic and intestinal organoids

We found that amino-acid starvation mainly impacted peroxisomes in hepatic organoids, whereas both peroxisomes and mitochondria were affected in intestinal organoids. The disparate impact on mitochondria plausibly reflects metabolic differences between the intestine and the liver. In the liver mitochondria are important for fatty acid oxidation, whereas in the intestine mitochondria are essential for proper stem cell function and thereby epithelial turnover[27,60]. In addition, nutrient requirements may be higher in the intestine due to the high turnover rate, which could lead to more severe mitochondrial changes when exposed to a similar nutritional insult.

In starved hepatic organoids we found that peroxisomal marker proteins were significantly decreased, which corresponded to reduced peroxisomal numbers in the liver of low-protein fed rodents[29,30]. It has been shown that peroxisomes are selectively degraded upon amino acid starvation[61,62]. Reduction of peroxisomal proteins is in line with the observed accumulation of phytanic acid and VLCFA in the starved organoids. Phytanic acid is a branched-chain fatty acid and substrate for the peroxisomal α-oxidation, whereas VLCFA are substrates for the peroxisomal β-oxidation[63]. Mitochondrial marker proteins were unaffected in starved hepatic organoids, which was very similar in rats that were fed a low protein diet for 1 week[30]. However, after 4 weeks mitochondria had an aberrant structure and compromised fatty-acid β-oxidation in these animals, which together with a decline in peroxisomal number was thought to contribute to the observed hepatic steatosis[30]. Likewise, we found that starved hepatic organoids were more prone to accumulate fat than their healthy counterparts, although the increase in TG was relatively small. Interestingly, mitochondrial oxygen consumption was not significantly affected in hepatic organoids starved for 48 hours, which was different from decreased mitochondrial respiration reported in low-protein fed rats after 4 weeks[30]. This may be attributed to differences between model systems (e.g. in vivo versus in vitro) and experimental design (e.g. isolated mitochondria versus whole-organoids respirometry). Alternatively, it has been suggested that peroxisome decline precedes mitochondrial decline[30], which is consistent with findings that defects in peroxisome biogenesis cause mitochondrial decline[64]. Possibly, the 48 hours of starvation of hepatic organoids represents earlier events in the progression of the phenotype than the 4 weeks of low-protein feeding in rats.

In starved intestinal organoids both mitochondrial membrane and matrix markers were lower, reminiscent of reduced mitochondrial numbers in the intestine of mice on a low protein diet (Chapter 5). The decline of peroxisomal marker proteins in intestinal organoids is a novel finding for the intestine and interestingly, seemed more severe in intestinal organoids than in hepatic organoids. As mitochondria play an important role in maintaining the stem cell niche[27,60], the reduction in mitochondrial markers proteins could contribute to the observed crypt atrophy in the organoids. Although peroxisomes are highly abundant in the small intestine[65], little is known about the functional significance of these organelles in this organ. In Drosophila, peroxisomes are required for homeostasis of intestinal epithelium[66]. More recently, Du et al. reported that elevated peroxisome numbers are required for stem cell differentiation and epithelial repair in human, mouse and Drosophila intestine[42]. Reduced or dysfunctional peroxisomes could result in epithelial instability[66] via redox stress, and compromise epithelial turnover[42]. Intestinal organoids are a versatile model to further explore the reduction of peroxisomes upon amino-acid starvation and its consequences for intestinal homeostasis.

Translation into potential treatments for severely malnourished children

We tested if targeting mitochondria and peroxisomes could preserve organ homeostasis under amino- acid deprived conditions. In starved hepatic organoids, addition of PPARα agonist fenofibrate reduced the accumulation of phytanic acid and very long chain fatty acids. In contrast, fenofibrate treatment in low-protein fed rats significantly improved mitochondrial β-oxidation capacity resulting in reduced hepatic fat deposition[30]. The positive effect on peroxisomes offers therapeutic potential[45]. Fenofibrate is usually well-tolerated during treatment of dyslipidemia, but side effects such as rhabdomyolysis are a risk in severely malnourished children[67]. Further investigation is required into the mechanisms of action, into the later effects of malnutrition on the mitochondria, and into the possibilities of PPARα-modulating dietary components (e.g. polysaturated fatty acids, flavonoids) in improving hepatic function in severe malnutrition[68,69].

In starved intestinal organoids, rapamycin preserved mitochondria and peroxisomes. This coincided with higher levels of tight junction protein claudin-3 than in starved, untreated organoids, suggesting better maintained barrier function. Leakage of FITC into the lumen in rapamycin-administered organoids was barely affected, but additional biological replicates are required. Accumulating data suggests a key role for mitochondria in maintaining the intestinal barrier[26], but for peroxisomes this is less known. Improved

mitochondrial health may be attributed to stimulated mitochondrial biogenesis, as PGC1-α protein levels were increased in rapamycin-administered starved organoids. In addition, rapamycin could improve mitochondrial homeostasis via clearance of dysfunctional mitochondria through autophagy activation[70], thereby contributing to the potentially improved barrier function. The potential positive impact of rapamycin on the intestinal barrier has therapeutic implications for severely malnourished children, because it could have potential to prevent bacterial translocation-induced clinical deterioration and death[57–59].

In conclusion, the results support the notion that hepatic and intestinal organoid models can be used to further investigate underlying mechanisms of organ dysfunction in severe malnutrition as well as to explore therapeutic interventions.

Acknowledgements

We would like to thank Karen van Eunen, Niels Kloosterhuis and Marieke Smit for their technical support with intestinal organoids and animal work. We would also like to acknowledge Hans Clevers, Tomohiro Mizutani, Jeroen Korving and Klaas Nico Faber for their advice on culturing of organoids. This project has received funding from the European Union's Horizon 2020 research and innovation programme under the Marie Skłodowska-Curie grant agreement No 812968. CJV received an MD-PhD fellowship from the University Medical Center Groningen and financial support from Stichting De Cock-Hadders. This work is further supported by the Canadian Institutes of Health Research (156307).

References

1. Sato T, Vries RG, Snippert HJ, van de Wetering M, Barker N, Stange DE, et al. Single Lgr5 stem cells build crypt-villus structures in vitro without a mesenchymal niche. Nature. 2009;459(7244):262–5.
2. Huch M, Dorrell C, Boj SF, van Es JH, Li VSW, van de Wetering M, et al. In vitro expansion of single Lgr5+ liver stem cells induced by Wnt-driven regeneration. Nature. 2013;494(7436):247–50.
3. Huch M, Koo B-K. Modeling mouse and human development using organoid cultures. Development. 2015;142(18):3113–25.
4. Dutta D, Heo I, Clevers H. Disease Modeling in Stem Cell-Derived 3D Organoid Systems. Trends Mol Med. 2017;23(5):393–410.
5. Clevers H. Modeling Development and Disease with Organoids. Cell. 2016;165(7):1586–97.
6. Okkelman IA, Neto N, Papkovsky DB, Monaghan MG, Dmitriev RI. A deeper understanding of intestinal organoid metabolism revealed by combining fluorescence lifetime imaging microscopy (FLIM) and extracellular flux analyses. Redox Biol. 2020;30:101420.
7. Kruitwagen HS, Oosterhoff LA, Vernooij IGWH, Schrall IM, van Wolferen ME, Bannink F, et al. Long-Term Adult Feline Liver Organoid Cultures for Disease Modeling of Hepatic Steatosis. Stem cell reports. 2017;8(4):822–30.
8. Cai T, Qi Y, Jergens A, Wannemuehler M, Barrett TA, Wang Q. Effects of six common dietary nutrients on murine intestinal organoid growth. PLoS One. 2018;13(2):e0191517.
9. Chen Y, Michalak M, Agellon LB. Importance of Nutrients and Nutrient Metabolism on Human Health. Yale J Biol Med. 2018;91(2):95–103.
10. André Briend PhD MD. Kwashiorkor: still an enigma – the search must go on [Internet]. Emergency Nutrition Network (ENN); 2014. Available from: https://www.ennonline.net/kwashiorkorstillanenigma
11. Attia S, Versloot CJ, Voskuijl W, van Vliet SJ, Di Giovanni V, Zhang L, et al. Mortality in children with complicated severe acute malnutrition is related to intestinal and systemic inflammation: an observational cohort study. Am J Clin Nutr. 2016;104(5):1441–9.
12. Kerac M, Bunn J, Chagaluka G, Bahwere P, Tomkins A, Collins S, et al. Follow-up of post-discharge growth and mortality after treatment for severe acute malnutrition (FuSAM study): a prospective cohort study. PLoS One. 2014;9(6):e96030.
13. Munthali T, Jacobs C, Sitali L, Dambe R, Michelo C. Mortality and morbidity patterns in under-five children with severe acute malnutrition (SAM) in Zambia: a five-year retrospective review of hospital-based records (2009-2013). Arch Public Health. 2015;73(1):23.
14. Ubesie AC, Ibeziako NS, Ndiokwelu CI, Uzoka CM, Nwafor CA. Under-five protein energy malnutrition admitted at the University of Nigeria Teaching Hospital, Enugu: a 10 year retrospective review. Nutr J. 2012;11:43.
15. Wharton B. Hypoglycaemia in children with kwashiorkor. Lancet. 1970;1(7639):171–3.
16. Nduhukire T, Atwine D, Rachel L, Byonanebye JE. Predictors of in-hospital mortality among under-five children with severe acute malnutrition in South-Western Uganda. PLoS One. 2020;15(6):e0234343.
17. Bandsma RHJ, Mendel M, Spoelstra MN, Reijngoud D-J, Boer T, Stellaard F, et al. Mechanisms behind decreased endogenous glucose production in malnourished children. Pediatr Res. 2010;68(5):423–8.

18. Grenov B, Lanyero B, Nabukeera-Barungi N, Namusoke H, Ritz C, Friis H, et al. Diarrhea, Dehydration, and the Associated Mortality in Children with Complicated Severe Acute Malnutrition: A Prospective Cohort Study in Uganda. J Pediatr. 2019;210:26–33.
19. Badaloo A V, Forrester T, Reid M, Jahoor F. Lipid kinetic differences between children with kwashiorkor and those with marasmus. Am J Clin Nutr. 2006 Jun;83(6):1283–8.
20. Badaloo A, Reid M, Soares D, Forrester T, Jahoor F. Relation between liver fat content and the rate of VLDL apolipoprotein B-100 synthesis in children with protein-energy malnutrition. Am J Clin Nutr. 2005;81(5):1126–32.
21. Brooks SE, Goldon MH, Taylor E. Hepatic ultrastructure in children with protein-energy malnutrition. West Indian Med J. 1992;41(4):139–45.
22. Shiner M, Redmond AO, Hansen JD. The jejunal mucosa in protein-energy malnutrition. A clinical, histological, and ultrastructural study. Exp Mol Pathol. 1973;19(1):61–78.
23. Campos J V, Neto UF, Patricio FR, Wehba J, Carvalho AA, Shiner M. Jejunal mucosa in marasmic children. Clinical, pathological, and fine structural evaluation of the effect of protein-energy malnutrition and environmental contamination. Am J Clin Nutr. 1979;32(8):1575–91.
24. Brunser O, Castillo C, Araya M. Fine structure of the small intestinal mucosa in infantile marasmic malnutrition. Gastroenterology. 1976;70(4):495–507.
25. Theron JJ, Wittmann W, Prinsloo JG. The fine structure of the jejunum in kwashiorkor. Exp Mol Pathol. 1971;14(2):184–99.
26. Rath E, Moschetta A, Haller D. Mitochondrial function - gatekeeper of intestinal epithelial cell homeostasis. Nat Rev Gastroenterol Hepatol. 2018;15(8):497–516.
27. Ludikhuize MC, Meerlo M, Gallego MP, Xanthakis D, Burgaya Julià M, Nguyen NTB, et al. Mitochondria Define Intestinal Stem Cell Differentiation Downstream of a FOXO/Notch Axis. Cell Metab. 2020;32(5):889-900.e7.
28. Lopes F, Keita Å V, Saxena A, Reyes JL, Mancini NL, Al Rajabi A, et al. ER-stress mobilization of death-associated protein kinase-1-dependent xenophagy counteracts mitochondria stress-induced epithelial barrier dysfunction. J Biol Chem. 2018;293(9):3073–87.
29. Sargent G, van Zutphen T, Shatseva T, Zhang L, Di Giovanni V, Bandsma R, et al. PEX2 is the E3 ubiquitin ligase required for pexophagy during starvation. J Cell Biol. 2016;214(6):677–90.
30. van Zutphen T, Ciapaite J, Bloks VW, Ackereley C, Gerding A, Jurdzinski A, et al. Malnutrition-associated liver steatosis and ATP depletion is caused by peroxisomal and mitochondrial dysfunction. J Hepatol. 2016;65(6):1198–208.
31. Johnson MA, Vidoni S, Durigon R, Pearce SF, Rorbach J, He J, et al. Amino acid starvation has opposite effects on mitochondrial and cytosolic protein synthesis. PLoS One. 2014;9(4):e93597.
32. Fabris G, Dumortier O, Pisani DF, Gautier N, Van Obberghen E. Amino acid-induced regulation of hepatocyte growth: possible role of Drosha. Cell Death Dis. 2019;10(8):566.
33. Hu H, Gehart H, Artegiani B, LÖpez-Iglesias C, Dekkers F, Basak O, et al. Long-Term Expansion of Functional Mouse and Human Hepatocytes as 3D Organoids. Cell. 2018;175(6):1591-1606.e19.
34. Zachos NC, Kovbasnjuk O, Foulke-Abel J, In J, Blutt SE, de Jonge HR, et al. Human Enteroids/Colonoids and Intestinal Organoids Functionally Recapitulate Normal Intestinal Physiology and Pathophysiology. J Biol Chem. 2016;291(8):3759–66.
35. Broutier L, Andersson-Rolf A, Hindley CJ, Boj SF, Clevers H, Koo B-K, et al. Culture and establishment of self-renewing human and mouse adult liver and pancreas 3D organoids and their genetic manipulation. Nat Protoc. 2016;11(9):1724–43.

36. Evers B, Gerding A, Boer T, Heiner-Fokkema MR, Jalving M, Wahl SA, et al. Simultaneous Quantification of the Concentration and Carbon Isotopologue Distribution of Polar Metabolites in a Single Analysis by Gas Chromatography and Mass Spectrometry. Anal Chem. 2021;93(23):8248–56.
37. Heberle AM, Razquin Navas P, Langelaar-Makkinje M, Kasack K, Sadik A, Faessler E, et al. The PI3K and MAPK/p38 pathways control stress granule assembly in a hierarchical manner. Life Sci alliance. 2019 Apr;2(2).
38. Thacker JS, Yeung DH, Staines WR, Mielke JG. Total protein or high-abundance protein: Which offers the best loading control for Western blotting? Anal Biochem. 2016;496:76–8.
39. Brown EM, Wlodarska M, Willing BP, Vonaesch P, Han J, Reynolds LA, et al. Diet and specific microbial exposure trigger features of environmental enteropathy in a novel murine model. Nat Commun. 2015;6:7806.
40. Huang T-Y, Zheng D, Houmard JA, Brault JJ, Hickner RC, Cortright RN. Overexpression of PGC-1α increases peroxisomal activity and mitochondrial fatty acid oxidation in human primary myotubes. Am J Physiol Endocrinol Metab. 2017;312(4):E253–63.
41. Imanaka T, Aihara K, Suzuki Y, Yokota S, Osumi T. The 70-kDa peroxisomal membrane protein (PMP70), an ATP-binding cassette transporter. Cell Biochem Biophys. 2000;32:131–8.
42. Du G, Xiong L, Li X, Zhuo Z, Zhuang X, Yu Z, et al. Peroxisome Elevation Induces Stem Cell Differentiation and Intestinal Epithelial Repair. Dev Cell. 2020;53(2):169-184.e11.
43. Wada Y, Takeda Y, Kuwahata M. Potential Role of Amino Acid/Protein Nutrition and Exercise in Serum Albumin Redox State. Nutrients. 2017;10(1).
44. Morlese JF, Forrester T, Badaloo A, Del Rosario M, Frazer M, Jahoor F. Albumin kinetics in edematous and nonedematous protein-energy malnourished children. Am J Clin Nutr. 1996;64(6):952–9.
45. Williams CD. A nutritional disease of childhood associated with a maize diet. Arch Dis Child. 1933;8(48):423–33.
46. Hu G, Ling C, Lijun C, Furse S, Koulman A, Swann J. The role of the tryptophan-nicotinamide pathway in a model of severe malnutrition induced liver dysfunction. Submitted. 2021;
47. Cassim S, Raymond V-A, Lapierre P, Bilodeau M. From in vivo to in vitro: Major metabolic alterations take place in hepatocytes during and following isolation. PLoS One. 2017;12(12):e0190366.
48. Nagarajan SR, Paul-Heng M, Krycer JR, Fazakerley DJ, Sharland AF, Hoy AJ. Lipid and glucose metabolism in hepatocyte cell lines and primary mouse hepatocytes: a comprehensive resource for in vitro studies of hepatic metabolism. Am J Physiol Endocrinol Metab. 2019;316(4):E578–89.
49. Peng WC, Logan CY, Fish M, Anbarchian T, Aguisanda F, Álvarez-Varela A, et al. Inflammatory Cytokine TNFα Promotes the Long-Term Expansion of Primary Hepatocytes in 3D Culture. Cell. 2018;175(6):1607-1619.e15.
50. Moore SR, Guedes MM, Costa TB, Vallance J, Maier EA, Betz KJ, et al. Glutamine and alanyl-glutamine promote crypt expansion and mTOR signaling in murine enteroids. Am J Physiol Gastrointest Liver Physiol. 2015;308(10):G831-9.
51. Saito Y, Iwatsuki K, Hanyu H, Maruyama N, Aihara E, Tadaishi M, et al. Effect of essential amino acids on enteroids: Methionine deprivation suppresses proliferation and affects differentiation in enteroid stem cells. Biochem Biophys Res Commun. 2017;488(1):171–6.
52. Richmond CA, Shah MS, Carlone DL, Breault DT. An enduring role for quiescent stem cells. Dev Dyn. 2016;245(7):718–26.
53. Buczacki SJA, Zecchini HI, Nicholson AM, Russell R, Vermeulen L, Kemp R, et al. Intestinal label-

retaining cells are secretory precursors expressing Lgr5. Nature. 2013;495(7439):65–9.

54. van Es JH, Sato T, van de Wetering M, Lyubimova A, Yee Nee AN, Gregorieff A, et al. Dll1+ secretory progenitor cells revert to stem cells upon crypt damage. Nat Cell Biol. 2012;14(10):1099–104.
55. Tetteh PW, Basak O, Farin HF, Wiebrands K, Kretzschmar K, Begthel H, et al. Replacement of Lost Lgr5-Positive Stem Cells through Plasticity of Their Enterocyte-Lineage Daughters. Cell Stem Cell. 2016;18(2):203–13.
56. Jadhav U, Saxena M, O'Neill NK, Saadatpour A, Yuan G-C, Herbert Z, et al. Dynamic Reorganization of Chromatin Accessibility Signatures during Dedifferentiation of Secretory Precursors into Lgr5+ Intestinal Stem Cells. Cell Stem Cell. 2017;21(1):65-77.e5.
57. Amadi B, Besa E, Zyambo K, Kaonga P, Louis-Auguste J, Chandwe K, et al. Impaired Barrier Function and Autoantibody Generation in Malnutrition Enteropathy in Zambia. EBioMedicine. 2017;22:191–9.
58. Farràs M, Chandwe K, Mayneris-Perxachs J, Amadi B, Louis-Auguste J, Besa E, et al. Characterizing the metabolic phenotype of intestinal villus blunting in Zambian children with severe acute malnutrition and persistent diarrhea. PLoS One. 2018;13(3):e0192092.
59. Boaz RT, Joseph AJ, Kang G, Bose A. Intestinal permeability in normally nourished and malnourished children with and without diarrhea. Indian Pediatr. 2013;50(1):152–3.
60. Khaloian S, Rath E, Hammoudi N, Gleisinger E, Blutke A, Giesbertz P, et al. Mitochondrial impairment drives intestinal stem cell transition into dysfunctional Paneth cells predicting Crohn's disease recurrence. Gut. 2020;69(11):1939–51.
61. Hara-Kuge S, Fujiki Y. The peroxin Pex14p is involved in LC3-dependent degradation of mammalian peroxisomes. Exp Cell Res. 2008;314(19):3531–41.
62. Jiang L, Hara-Kuge S, Yamashita S-I, Fujiki Y. Peroxin Pex14p is the key component for coordinated autophagic degradation of mammalian peroxisomes by direct binding to LC3-II. Genes Cells. 2015;20(1):36–49.
63. Wanders RJA, Komen J, Ferdinandusse S. Phytanic acid metabolism in health and disease. Biochim Biophys Acta. 2011;1811(9):498–507.
64. Peeters A, Shinde AB, Dirkx R, Smet J, De Bock K, Espeel M, et al. Mitochondria in peroxisome-deficient hepatocytes exhibit impaired respiration, depleted DNA, and PGC-1α independent proliferation. Biochim Biophys Acta. 2015;1853(2):285–98.
65. Roels F, Espeel M, Pauwels M, De Craemer D, Egberts HJ, van der Spek P. Different types of peroxisomes in human duodenal epithelium. Gut. 1991 Aug;32(8):858–65.
66. Di Cara F, Bülow MH, Simmonds AJ, Rachubinski RA. Dysfunctional peroxisomes compromise gut structure and host defense by increased cell death and Tor-dependent autophagy. Mol Biol Cell. 2018;29(22):2766–83.
67. Kiskac M, Zorlu M, Cakirca M, Karatoprak C, Peru C, Erkoc R, et al. A case of rhabdomyolysis complicated with acute renal failure after resumption of fenofibrate therapy: a first report. Indian J Pharmacol. 2013;45(3):305–6.
68. Rigano D, Sirignano C, Taglialatela-Scafati O. The potential of natural products for targeting PPARα. Acta Pharm Sin B. 2017;7(4):427–38.
69. Keller H, Dreyer C, Medin J, Mahfoudi A, Ozato K, Wahli W. Fatty acids and retinoids control lipid metabolism through activation of peroxisome proliferator-activated receptor-retinoid X receptor heterodimers. Proc Natl Acad Sci U S A. 1993;90(6):2160–4.
70. Bartolomé A, García-Aguilar A, Asahara S-I, Kido Y, Guillén C, Pajvani UB, et al. MTORC1 Regulates both General Autophagy and Mitophagy Induction after Oxidative Phosphorylation Uncoupling. Mol Cell Biol. 2017;37(23).

Supplementary data

Supplementary Figure 1. Relative gene expression of stem cell markers and hepatocyte markers in liver progenitor organoids and mature hepatic organoids.

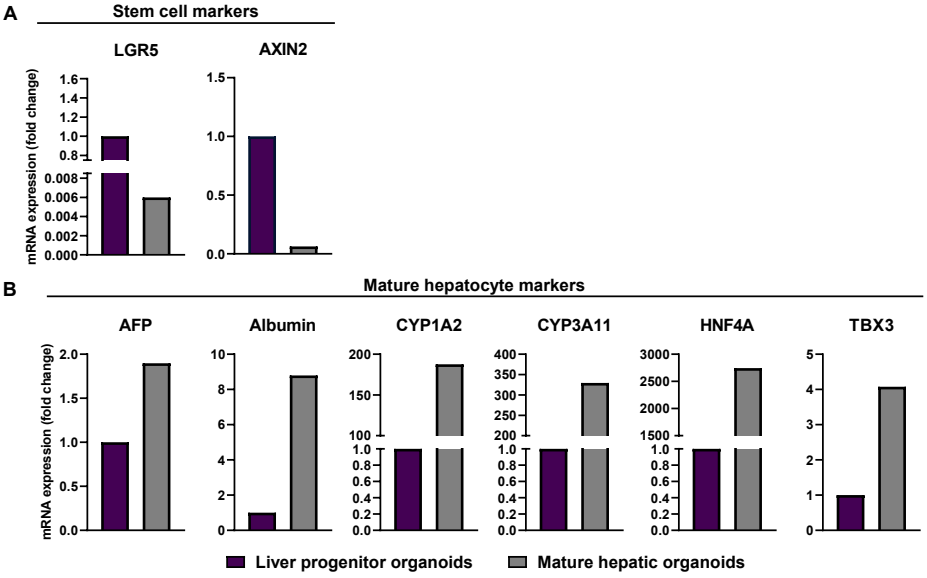

Relative gene expression of stem cells markers (**A**) and mature hepatocyte markers (**B**) measured in liver progenitor organoids and differentiated mature hepatic organoids. Liver progenitor organoids expressed stem cell markers (LGR5, AXIN2) while differentiated mature hepatic organoids expressed early and mature hepatocyte markers (e.g. HNF4A, CYP1A2). Data represent 1 biological replicate.

Supplementary Figure 2. Organoid size and growth rate of liver progenitor organoids cultured in control and amino-acid-free medium.

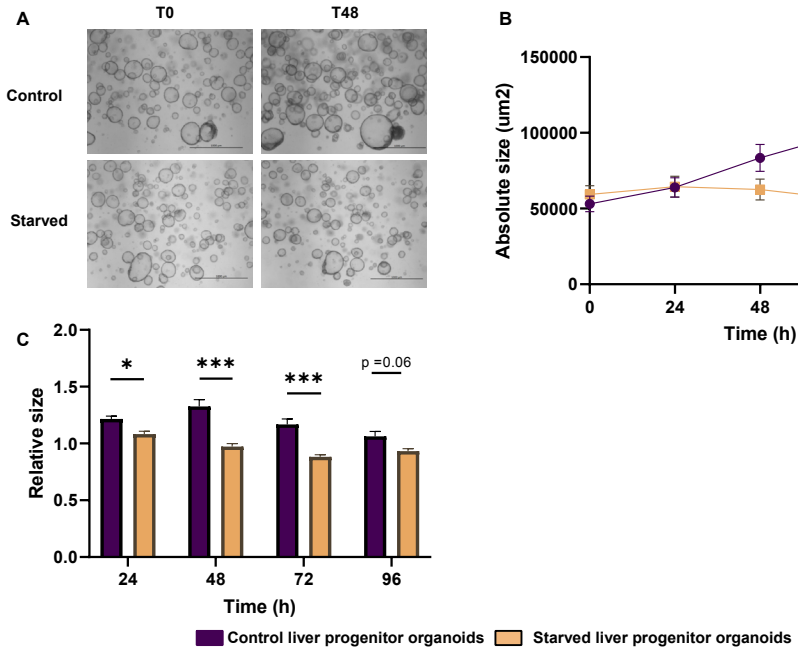

(A) Representative images of liver progenitor organoids that were grown in complete culture medium (control) or amino-acid-free medium (starved) for 48 hours. Scale bar, 1000 µm. **(B)** Organoid size over time of control and starved organoids. Data represents 1 biological replicate, error bars indicate the SEM. (*** P<0.001, repeated measures analysis of variance). **(C)** Relative size expressed as size of an organoid at time point of interest divided by the size of the same organoid 24 hours earlier, calculated for 25 random organoids. Data represents 1 biological replicate, error bars indicate the SEM (*P<0.05, *** P<0.001, repeated measures analysis of variance).

Supplementary Figure 3. Organoid size and number of crypts per organoid.

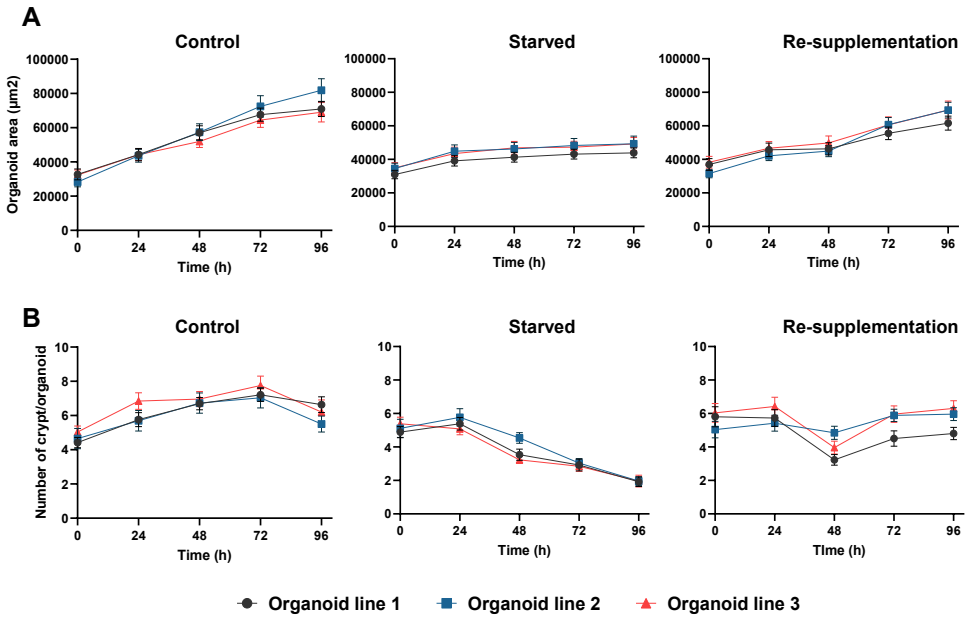

Organoids were grown in complete culture medium (control), amino-acid-free medium (starved), amino-acid-free medium for 48 h followed by complete culture medium for 48 h (re-supplementation). (**A**) The size of 26 organoids was measured every 24 hours for each experimental condition in 3 different organoid lines. (**B**) In addition, the number of crypts per organoid were assessed in the organoids that were measured in (A).

Supplementary Figure 4. Relative gene expression markers for stem cells, proliferation and differentiation in intestinal organoids.

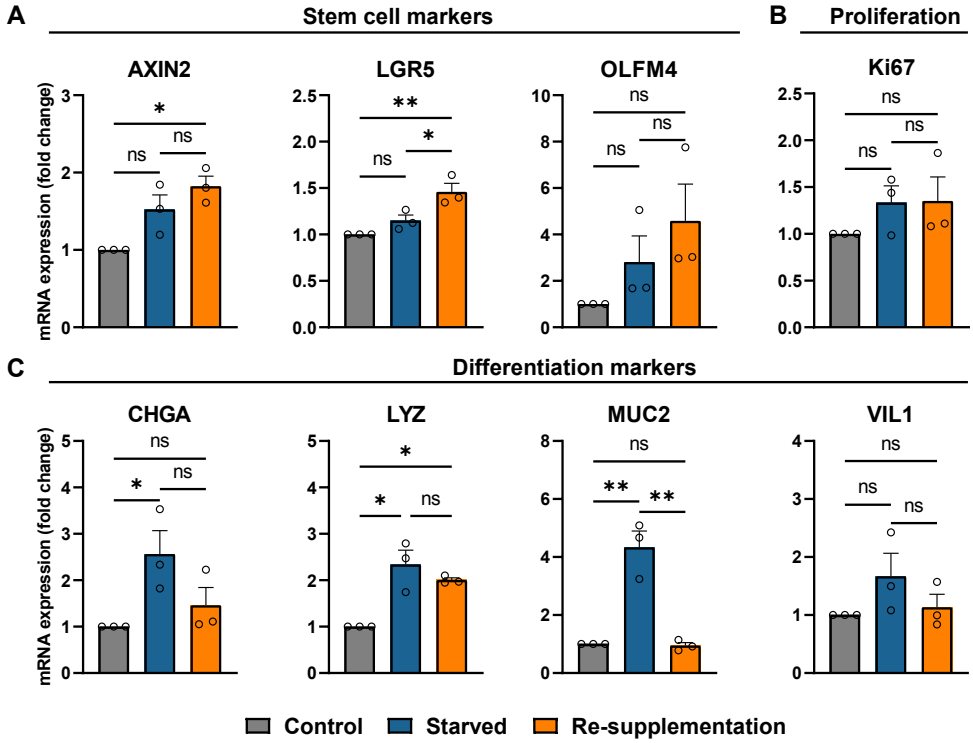

Relative gene expression of stem cells markers (**A**), proliferation markers (**B**) and markers of differentiation (**C**) measured in intestinal organoids grown in complete culture medium (control), amino-acid-free medium (starved) or amino-acid-free medium for 48 h followed by complete culture medium for 48 h (re-supplementation). Data represents 3 biological replicates (* P<0.05, ** P<0.01, Two-way ANOVA with Tukey's post hoc test). AXIN2, axis inhibition protein 2; LGR5, Leucine Rich Repeat Containing G Protein-Coupled Receptor 5; OLFM4, olfactomedin 4; CHGA, chromogranin A; LYZ, lysozyme; MUC2, mucin-2; VIL1, villin 1.

Supplementary Figure 5. FITC fluorescence in the lumen of intestinal organoids.

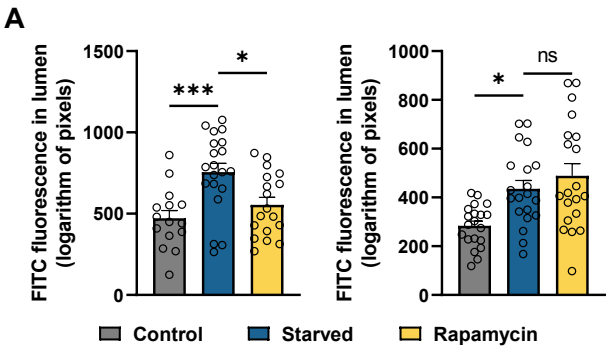

FITC fluorescence was measured in the lumen of intestinal organoids that were grown in complete culture medium (control), amino-acid-free medium (starved) and amino-acid-free medium supplemented with 2nM rapamycin (rapamycin). Graphs represent two different organoid lines. Data points are individual organoids random selected by a random generator and the error bars indicate the SEM (*P <0.05, *** P<0.001, two-way ANOVA with Tukey's post hoc test).

Supplementary Table 1. List of primer sequences used in RT-qPCR.

Gene Name	Forward and reverse primer sequence (5'- 3')
PPIA	Fwd: TTCCTCCTTTCACAGAATTATTCCA Rev: CCGCCAGTGCCATTATGG
LGR5	Fwd: GGAAATGCTTTGACACACATTC Rev: GGAAGTCATCAAGGTTATTATAA
AXIN2	Fwd: TAAGCAGCCGTTCGCGATG Rev: TTCTTCCAGTTCCTCTCAG
Ki67	Fwd: ATCATTGACCGCTCCTTTAGGT Rev: GCTCGCCTTGATGGTTCCT
HNF4-a	Fwd: GCTAAGGCGTGGGTAGGG Rev: AGGCTGTTGGATGAATTGAGG
AFP	Fwd: CCAGGAAGTCTGTTTCACAGAAG Rev: CAAAAGGCTCACACCAAAGAG
CYP1a2	Fwd: TTCAGTCCCTCCTTACAGCC Rev: TCCAAGGCAGAATACGGTGAC
CYP3a11	Fwd: TGGTCAAACGCCTCTCCTTGCTG Rev: ACTGGGCCAAAATCCCGCCG
TBX3	Fwd: GAGGCCAAGGAACTTTGGGA Rev: AGGGAACATTCGCCTTCCTG
Catalase	Fwd: AGCGACCAGATGAAGCAGTG Rev: TCCGCTCTCTGTCAAAGTGTG
ACOX1	Fwd: TAACTTCCTCACTCGAAGCCA Rev: AGTTCCATGACCCATCTCTGTC
Albumin	Fwd: GCGCAGATGACAGGGCGGAA Rev: GTGCCGTAGCATGCGGGAGG
VIL1	Fwd: GCTTGCCACAACTTCCTAAGAT Rev: TCAGTTTAGTCATGGTGGACGA
MUC2	Fwd: TGTGGAACCGGGAAGATG Rev: GACCACAGGTATGGTTCTGGA
CHGRA	Fwd: CGATCCAGAAAGATGATGGTC Rev: CGGAAGCCTCTGTCTTTCC
OLFM4	Fwd: AGAAATCGTGGCTCTGAAG Rev: GTTCACCACACCACCATGAC
LYZ1	Fwd: AGACCGAAGCACCGACTATG Rev: CGGTTTTGACATTGTGTTCG

Fwd, forward primer; Rev, reverse primer.

Supplementary Table 2. List of primary antibodies used in immunoblotting.

Name	Company	Category number	Dilution
ACOX1	Abcam	Ab184032	1:1000
B-actin	Sigma-Aldrich	A5441	1:1000
Catalase	Santa Cruz	SC-271803	1:1000
Claudin-3	Thermo Fisher Scientific	54481	1:2000
HSP60	Cell Signaling	4870S	1:1000
PGC1α	Abcam	54481	1:1000
PMP70	Sigma-Aldrich	P0497	1:1000
TOM20	Cell Signaling	D8T4N	1:1000
Total OXPHOS	Abcam	110413	1:1000

Supplementary Table 3. Amino acid concentrations measured in the medium of mature hepatic organoids.

	Concentration (μM)	
Amino acid	**Control medium**	**Amino-acid-starvation medium**
Alanine	1405 ± 110	86 + 19
Asparagine	32 ± 8	7.0 ± 0.2
Glutamic Acid	136 ± 169	166 ± 233
Glutamine	480 ± 164	10 ± 1
Glycine	144 ± 3	5 ± 0.1
Isoleucine	328 ± 11	8 ± 2
Leucine	327 ± 9	10 ± 2
Lysine	284 ± 26	16 ± 4
Phenylalanine	188 ± 10	10 ± 2
Proline	162 ± 22	41 ± 5
Serine	147 ± 9	2 ± 0
Tyrosine	151 ± 10	14 ± 1
Valine	410 ± 3	18 ± 4

Amino acid concentrations were measured in medium that had been in the well with organoids for 48 hours. Data is expressed as mean ± SD and represents 3 biological replicates for control medium and 2 biological replicates for amino-acid-starvation medium.

PART III

FUTURE PERSPECTIVES